Effects of Cu doping on thermoelectric properties of Al–Si–Ru semiconducting quasicrystalline approximant

Yutaka Iwasaki,[1,*] Koichi Kitahara,[1,2] and Kaoru Kimura[1,2]

[1]*Department of Advanced Materials Science, The University of Tokyo, 5-1-5 Kashiwanoha, Kashiwa, Chiba 277-8561, Japan*

[2]*AIST–UTokyo, Advanced Operando-Measurement Technology Open Innovation Laboratory (OPERANDO–OIL), National Institute of Advanced Industrial Science and Technology (AIST), 148 City Block 4, Kashiwanoha Campus, 178-4 Wakashiba, Kashiwa, Chiba 277-0871, Japan*

(Received 27 March 2021; accepted 23 November 2021; published 3 December 2021)

We have attempted to improve the thermoelectric performance of an Al–Si–Ru semiconducting approximant through optimizing the carrier concentration. The effects of Cu doping on the thermoelectric properties of an Al–Si–Ru semiconducting quasicrystalline approximant with the nominal composition of $Al_{69-0.75x}Si_{7.5}Cu_xRu_{23.5-0.25x}$ ($x = 0, 2, 4, 6, 8$) are investigated. At approximately room temperature, an increase of x leads to a decrease of the Seebeck coefficient S and an increase of the electrical conductivity. Density functional theory and the Boltzmann transport theory are used to calculate S as the hole concentration and the band gap are varied. The temperature dependence of S is quantitatively described by an increase of the hole concentration and narrowing of the band gap with increasing x. Cu doping is shown to increase the hole concentration and narrow the band gap. The maximum dimensionless figure of merit increases from 0.03 at 400 K for $x = 0$ to 0.2 at 500 K for $x = 4$. These results indicate that the semiconducting quasicrystalline approximant could be a suitable candidate as a thermoelectric material for low grade waste heat recovery.

DOI: 10.1103/PhysRevMaterials.5.125401

I. INTRODUCTION

Aluminum-based quasicrystals and their approximants, which have the same local structure as quasicrystals, are expected to exhibit a high thermoelectric performance because they usually possess semimetallic electrical properties owing to a deep pseudogap in the density of states and a low thermal conductivity that results from their complex structure [1–17]. The performance of thermoelectric materials is usually evaluated by the dimensionless figure of merit $zT = S^2\sigma T/(\kappa_{el} + \kappa_{lat})$, where S, σ, T, κ_{el}, and κ_{lat} are the Seebeck coefficient, electrical conductivity, absolute temperature, electronic thermal conductivity, and lattice thermal conductivity, respectively. The highest zT among quasicrystals achieved so far is 0.26 at 500 K in an Al–Ga–Pd–Mn quasicrystal [9], which is only a quarter of the general target value of unity. The main problem is that the value of S ($\approx$90 μV K^{-1}) is approximately half that of typical practical materials. To obtain a large S at a certain T, a semiconductor with a band gap of 6-10k_BT, where k_B is the Boltzmann constant, is usually required [18]. In the search for semiconducting quasicrystals, we have investigated semiconducting approximants. Because quasicrystalline approximants exhibit similar properties to quasicrystals, they are considered to be important materials for understanding the physical properties of quasicrystals [6,10,12]. While it is difficult to find semiconducting quasicrystals by calculating the band structure of quasicrystals using density functional theory (DFT) owing to their aperiodicity, it is possible to do so for approximants because of their periodicity. Therefore, the search for semiconducting quasicrystalline approximants can be a good approach to discover semiconducting quasicrystals. Recently, we have shown that the Al–Si–Ru 1/0 quasicrystalline approximant exhibits semiconducting properties with a band gap of approximately 0.15 eV [19]. However, the synthesized sample exhibited an intrinsic semiconducting behavior and quite a low maximum zT of 0.03 at 400 K because the carrier concentration was not optimized. Our previous study also suggested that the zT could reach a maximum of 0.7 at 500 K by optimizing the hole concentration. As a candidate for a hole dopant, we have focused on Cu with a valence number of +1, which can substitute for Al with a valence number +3 and is often used to determine the valence electron number of quasicrystals and their approximants [20]. According to previous reports [21,22], the binary Al–Ir and Al–Rh 1/0 quasicrystalline approximants, which are the same type of approximant as an Al–Si–Ru 1/0 quasicrystalline approximant, have a wide solubility limit ($\approx$15 at. %) of Cu. Furthermore, it has been reported that there is a 1/0 quasicrystalline approximant in the composition of $Al_{55.1}Si_{10.1}Cu_{14.6}Ru_{20.2}$ [23]. Therefore, the aim of the present work is to improve the thermoelectric performance of the Al–Si–Ru 1/0 quasicrystalline approximant by optimizing the carrier concentration through Cu doping.

II. EXPERIMENTAL AND CALCULATION METHOD

A. Sample preparation

Because the sample with a nominal composition of $Al_{67.6}Si_{8.9}Ru_{23.5}$, which was prepared in a previous study

*iwasaki@phys.mm.t.u-tokyo.ac.jp

 ©2021 American Physical Society

[19], had a poor reproducibility for obtaining a single phase, we found that a nominal composition of $Al_{69}Si_{7.5}Ru_{23.5}$ can reproduce a single phase well and adopted this as the base composition for the Cu doping samples. Synthesis of the single-phase Al–Si–Cu–Ru 1/0 quasicrystalline approximant samples was performed from commercial element powders, Al (3*N* purity; Kojundo Chemical Laboratory Co., Ltd., Japan), Si (4*N* purity; Kojundo Chemical Laboratory Co., Ltd., Japan), Cu (3*N* purity; Kojundo Chemical Laboratory Co., Ltd., Japan), and Ru (3*N* purity; Rare Metallic Co., Ltd., Japan) with a nominal composition of $Al_{69-0.75x}Si_{7.5}Cu_xRu_{23.5-0.25x}$ ($x = 0, 2, 4, 6, 8$). Note that we needed to substitute Cu for both Al and Ru in a 3:1 ratio, otherwise a secondary phase of $RuAl_2$ would appear. In this system, $RuAl_2$ phase contains several at. % Si and is an *n*-type semiconductor with a large negative Seebeck coefficient, which may negatively affect the thermoelectric properties of the matrix phase [24]. The mixed powders were pressed under 200 MPa into disk-shaped pellets. Each pellet was melted in an arc-melting furnace (NEV-ACD-05, NISSIN GIKEN Corporation, Japan) under an argon atmosphere. The weight loss of all the samples during arc melting was less than 1%. The ingots were wrapped in tantalum foil and sealed in a quartz tube filled with argon gas, followed by annealing at 1273 K for 72 h and water quenching. The annealed ingots were reground into powder and then sintered by spark plasma sintering (SPS) using a SPS apparatus (SPS-515S; Sumitomo Coal Mining Co., Ltd., Japan). The temperatures of the specimens were increased from room temperature to 1273 K, and then the samples were kept for 20 min at a uniaxial pressure of 90 MPa under an argon atmosphere. The sintered samples were annealed again under the same conditions as above. The relative density of each sintered bulk sample was greater than 95%.

B. Characterization

Phase identification was performed by x-ray diffraction (XRD) measurements with Cu K-$L_{2,3}$ radiation (Smart Lab; Rigaku Co., Japan). The lattice parameter a of each sample was refined by Le Bail analysis [25] using RIETAN-FP [26], and silicon powder was used as a line position standard (SRM640d; NIST, USA). Compositional analysis was performed by conventional scanning electron microprobe–energy dispersive x-ray spectroscopy (SEM–EDX) measurements (JSM-6010LA; JEOL Ltd., Japan) using the Al, Si, Cu, and Ru standards for EDX (JEOL Ltd., Japan). The true density was measured in a helium atmosphere with a multivolume pycnometer (AccuPyc 1330; Micrometrics, USA). The σ and S were measured in a helium atmosphere from 350 to 800 K by the four-probe method and the steady-state temperature gradient method, respectively, using a Seebeck coefficient/electric resistance measurement system (ZEM-1; Advance Riko, Inc., Japan). The speed of sound was measured by the ultrasonic pulse echo method using an echometer (Echometer 1062; Karl Deutsch Co., Germany). The thermal conductivity κ of the sample was measured using the laser flash method with a laser flash analysis apparatus (TC-7000, Advance Riko Co., Ltd.).

C. Calculation methods

The electronic structure was calculated by using the WIEN2k package, which is based on the full potential augmented plane wave + local orbitals method [27]. We note that the band gap E_g in the electronic structure used in the calculation of the thermoelectric properties was corrected as a parameter to describe the experimental results. The crystal structure of the calculated model $Al_{18}Si_5Ru_8$ and the conditions, such as the number of the **k**-mesh grid and energy cutoff constant used for the self-consistent-field calculation, have already been reported in our previous work [19]. The eigenenergy $\varepsilon_{n\mathbf{k}}$ and the group velocity $v_{n\mathbf{k}}$ on each **k** point were calculated on an unshifted $30 \times 30 \times 30$ **k**-mesh grid in the Brillouin zone. S and the Lorenz number L were then calculated in the same manner as described in Ref. [14] on the basis of the Boltzmann transport theory within the constant-diffusivity approximation, which has been frequently used to explain thermoelectric properties of quasicrystalline approximants [6,14,19]. This was expected to describe S and L of the approximants in a similar manner as quantum-mechanical transport theory that takes into account some non-Boltzmann contributions [17].

Here S and L are represented by following equations:

$$S = -\frac{1}{eT}\frac{\int \Xi(\varepsilon)\left(-\frac{df}{d\varepsilon}\right)(\varepsilon-\mu)d\varepsilon}{\int \Xi(\varepsilon)\left(-\frac{df}{d\varepsilon}\right)d\varepsilon}, \tag{1}$$

$$L = \frac{1}{e^2T^2}\frac{\int \Xi(\varepsilon)\left(-\frac{df}{d\varepsilon}\right)(\varepsilon-\mu)^2d\varepsilon}{\int \Xi(\varepsilon)\left(-\frac{df}{d\varepsilon}\right)d\varepsilon} - S^2, \tag{2}$$

$$\Xi(\varepsilon) \equiv \tfrac{1}{3}D(\varepsilon)v(\varepsilon)^2\tau(\varepsilon), \tag{3}$$

where e, T, ε, f, μ, $D(\varepsilon)$, $v(\varepsilon)$, and $\tau(\varepsilon)$ are the elemental charge, the absolute temperature, the energy, the Fermi-Dirac distribution function, the chemical potential, the density of states, the group velocity, and the relaxation time of electrons. Applying the constant diffusion coefficient approximation [$\Xi(\varepsilon) = D(\varepsilon)d_{\mathrm{el}}$, where d_{el} is the diffusion constant of electrons $d_{\mathrm{el}} = \frac{1}{3}v(\varepsilon)^2\tau(\varepsilon) = \mathrm{const.}$] to Eqs. (1) and (2), we obtain the following equations:

$$S = -\frac{1}{eT}\frac{\int D(\varepsilon)\left(-\frac{df}{d\varepsilon}\right)(\varepsilon-\mu)d\varepsilon}{\int D(\varepsilon)\left(-\frac{df}{d\varepsilon}\right)d\varepsilon}, \tag{4}$$

$$L = \frac{1}{e^2T^2}\frac{\int D(\varepsilon)\left(-\frac{df}{d\varepsilon}\right)(\varepsilon-\mu)^2d\varepsilon}{\int D(\varepsilon)\left(-\frac{df}{d\varepsilon}\right)d\varepsilon} - S^2. \tag{5}$$

Here we note that the magnitude of both S and L are independent from d_{el}.

III. RESULTS AND DISCUSSION

A. Structural properties

Figure 1 shows the XRD patterns for each Cu-doped sample. All of the diffraction peaks were indexed to the primitive cubic lattice with $a \approx 7.7$ Å, and no secondary phases were observed in any of the samples. The absence of any secondary phases was also observed in the SEM backscattered electron images. The analyzed composition obtained by EDX for each sample is shown in Table I. The analyzed compositions were almost the same as the nominal compositions for all

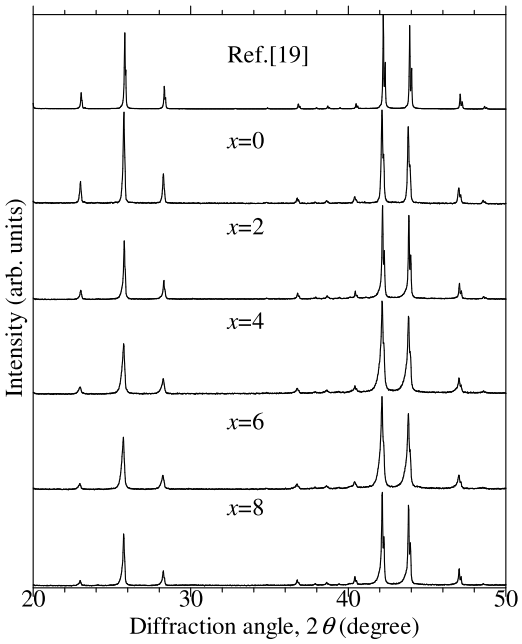

FIG. 1. XRD pattern of each synthesized sample with a nominal composition of $Al_{69-0.75x}Si_{7.5}Cu_xRu_{23.5-0.25x}$ ($x = 0$–8) together with a previously investigated sample [19].

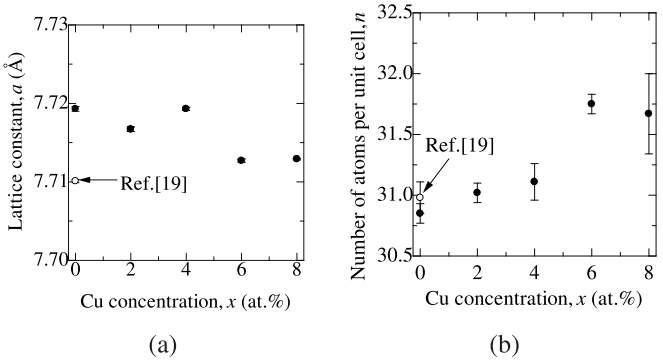

FIG. 2. (a) Lattice constant a and (b) number of atoms per unit cell n of each synthesized sample with a nominal composition of $Al_{69-0.75x}Si_{7.5}Cu_xRu_{23.5-0.25x}$ ($x = 0$–8) together with a previously investigated sample [19].

samples, although the analyzed compositions for several samples tended to be slightly Al poor and Si rich compared with the nominal compositions. The analyzed composition of Cu increased with increasing x, which indicated that the Cu was properly doped for all the samples. Figures 2(a) and 2(b), respectively, show a and the number of atoms per unit cell n, calculated by using a, the analyzed composition, and the true density as shown in Table I, as a function of x together with a previously investigated sample [19]. Even for the undoped samples ($x = 0$), a had a range of 0.01 Å from approximately 7.71 Å for the previous sample [19] to 7.72 Å for the present sample. The effect of Cu doping on a was well within the above range of 0.01 Å. Therefore, a is almost independent from x although the atomic radius of Cu is smaller than that of Al and Ru, assuming the atomic radii as Al: 0.143 nm, Cu: 0.128 nm, and Ru: 0.134 nm [28]. However, n increases with increasing x, which indicates that the doped Cu atoms are not only substituted for Al atoms but also add into interstitial sites. Such an interstitial Cu doping was also observed in our previous report regarding the Cu doping effect on an Al–Ir 1/0 quasicrystalline approximant [13]. Here the number of Al/Cu atoms in the cluster fluctuates from 10 to 12 for each unit cell. Therefore, the number of atoms in the cluster are averaged over 10 to 12 in an experimental bulk sample, so we can get n with noninteger values. These results suggest that the contribution of a decreasing, owing to the replacement of Al and Ru by Cu, and the contribution of a increasing, owing to the interstitial doping of Cu, cancel each other out, which results in a being independent of x.

B. Thermoelectric properties

Figures 3(a) and 3(b), respectively, show the T dependence of σ and S for a series of $Al_{69-0.75x}Si_{7.5}Cu_xRu_{23.5-0.25x}$ ($x = 0$–8) as well as a previously investigated sample [19]. The σ monotonically increased with increasing T for all the samples. While the undoped samples ($x = 0$ and previously investigated sample [19]) showed an intrinsic semiconducting trend, the Cu-doped samples ($x > 0$) showed a doped semiconducting trend. The S for the Cu-doped samples showed a maximum value in the range of 350 to 500 K and then decreased with increasing T at higher temperatures owing to bipolar diffusion. As x increased, the T at which S showed its maximum value shifted to a higher temperature and the maximum value of S decreased from approximately 170 to 85 μV K^{-1}. Over the entire investigated temperature range, σ increased with increasing x. Conversely, S monotonically decreased with increasing x near 350 K. Figure 3(b) also shows S calculated by using the parameters E_g and the number of holes per unit cell h shown in Fig. 3(c) for each sample.

TABLE I. Lattice constant, true density, speed of sound, and analyzed compositions for each element for the synthesized samples with a nominal composition of $Al_{69-0.75x}Si_{7.5}Cu_xRu_{23.5-0.25x}$ ($x = 0$–8).

Sample	Lattice constant (Å)	True density (g cm^{-3})	Speed of sound (km s^{-1})	Analyzed composition (at. %)			
				Al	Si	Cu	Ru
$x = 0$	7.7193(3)	4.95(1)	3.69	67.63(2)	8.2(2)	0	24.2(1)
$x = 2$	7.7167(3)	5.03(1)	3.72	66.5(9)	8.3(5)	2.2(3)	22.9(4)
$x = 4$	7.7193(2)	5.08(2)	3.26	65.6(3)	8.1(5)	4.1(5)	22.1(6)
$x = 6$	7.7127(2)	5.24(1)	3.57	64.5(4)	7.5(2)	6.0(5)	22.0(2)
$x = 8$	7.7129(1)	5.26(6)	3.76	62.5(3)	8.0(1)	8.4(3)	21.1(1)

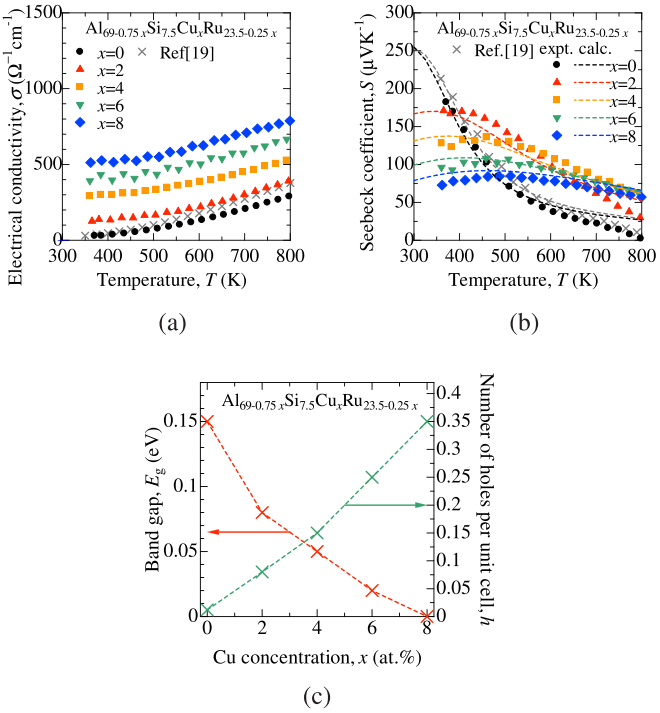

FIG. 3. Temperature T dependence of (a) the electrical conductivity σ and (b) the Seebeck coefficient S of each synthesized sample with a nominal composition of $Al_{69-0.75x}Si_{7.5}Cu_xRu_{23.5-0.25x}$ ($x = 0$–8) together with a previously investigated sample [19], where S calculated under the condition of (c) is also shown by a dashed line. (c) Band gap E_g and number of holes per unit cell h used for S calculated to reproduce the experimental S for each x.

The calculated S quantitatively described the experimental results for all the samples, which supported that E_g and h were reasonable values for each sample. h increased with increasing x, which indicated that the hole doping was successful. E_g decreased with increasing x, which indicated that the doped Cu narrowed E_g. Here one might think that even though the sample of $x = 8$ has no band gap, the temperature dependence of σ does not decrease with increasing temperature as seen in typical metals. However, in an electronic state with exactly zero band gap, such as the sample with $x = 8$, there is no density of states at the Fermi energy unlike in typical metals. Therefore, the temperature dependence of the carrier density behaves like a semiconductor, and the electrical conductivity also behaves like a semiconductor rather than typical metals. Such behavior is often observed in other quasicrystals with pseudogap [1–12].

To investigate the effect of doped Cu on the band structure, we calculated the band structure of $Al_{17}Si_5CuRu_8$, in which one Al was replaced by Cu in $Al_{18}Si_5Ru_8$ calculated in our previous work [19] and shown in Fig. 4 together with the Bloch orbital at the valence band maximum (VBM). Although the supercell method would usually be adopted to evaluate the effect of atomic substitution on the band structure, it is difficult to determine the band structure of the most stable structure using the supercell method because the approximant has a complex structure with large unit cell and the number of atoms per unit cell varies with Cu concentration on the

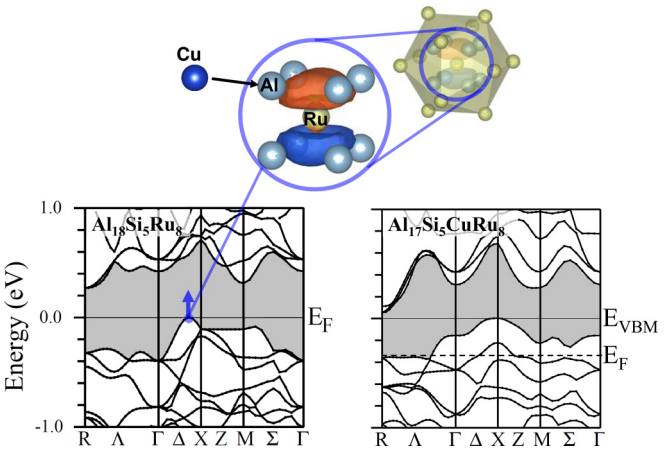

FIG. 4. Band structure of $Al_{18}Si_5Ru_8$ together with the Bloch orbital at the valence band maximum and $Al_{17}Si_5CuRu_8$.

experiment. Therefore, in this study, as a rough approximation, the symmetry of the unit cell was reduced from $Pm-3$ to $P1$, and one of the eight equivalent Al sites was replaced by Cu. In this case, the number of possible structural model patterns is only this one. This nonsupercell method has worked in our previous studies to qualitatively investigate the effect of Cu doping on band structure of an Al–Ir approximant [13]. Furthermore, we note that it is difficult to determine the atomic positions and occupancies of doped Cu atoms by structure refinement because the initial structure of the Al–Si–Ru 1/0 approximant, which is necessary for Rietveld analysis, has not yet been obtained by single crystal structure analysis. Instead of structure refinement, we discuss where the doped Cu occupies the sites from the model obtained by the single crystal structure analysis of the Al–Si–Cu–Ru 1/0 approximant solved by Sugiyama *et al.* [23], which contains more Cu (approximately 15 at. %) than our samples prepared in this study. The validity of where the doped Cu occupies is discussed in the Supplemental Materials [29]. The Cu-substituted band structure had a smaller E_g than the original band structure. This was proposed to arise from the VBM, which is dominated by sp orbitals of Al that are shifted upward by doped Cu so that it has a higher orbital energy than Al.

Figure 5(a) shows the T dependence of κ and κ_{lat} ($\equiv \kappa - \kappa_{el} = \kappa - L\sigma_{expt}T$) for $Al_{69-0.75x}Si_{7.5}Cu_xRu_{23.5-0.25x}$ ($x = 0$–8) as well as a previously investigated sample [19], where L is obtained by a DFT calculation with the same conditions as those shown in Fig. 3(c), which implicitly takes into account bipolar diffusion. The κ monotonically increased with increasing T for all the samples because of the increase of κ_{el}. The increasing trend in κ_{el} was not only owing to the increase in σ and T, but also owing to bipolar diffusion, because the L of each sample was larger than that of the degenerate limit at high temperature, as shown in Fig. 5(b). This was also consistent with the fact that the T at which L became larger than the value of the degenerate limit for each sample was almost equal to the T at which S started to decrease. However, κ_{lat} exhibited quite a low value of approximately 1.0 $W\,m^{-1}\,K^{-1}$ at room temperature in all samples probably because of the intrinsically complex crystal structure. For all the samples at high temperature, κ_{lat} reached the theoretical

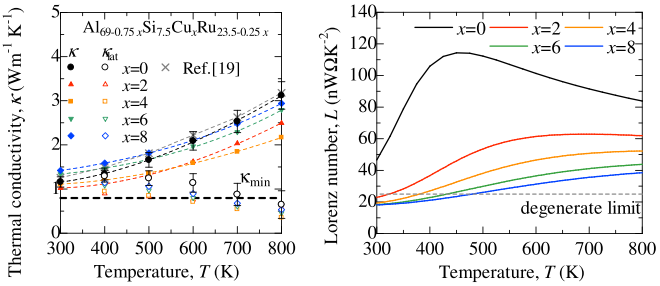

FIG. 5. Temperature T dependence of (a) the thermal conductivity κ and the lattice thermal conductivity $\kappa_{\rm lat}$ for a series of $Al_{69-0.75x}Si_{7.5}Cu_xRu_{23.5-0.25x}$ ($x = 0$–8) as well as a previously investigated sample [19] and (b) the calculated Lorenz number L with the same conditions as those shown in Fig. 3(c). Here, since the magnitude of error bar is almost same for each sample, it is only shown on the sample of $x = 0$ for improving visibility.

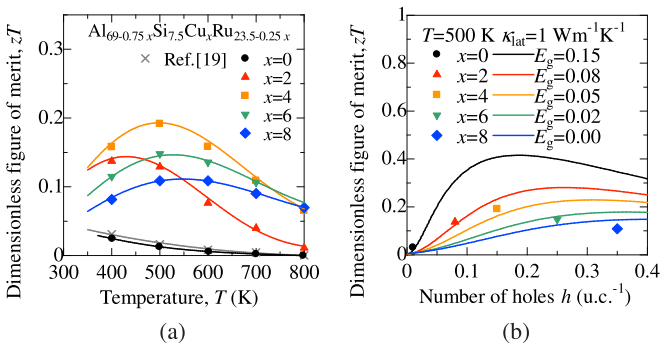

FIG. 6. (a) Temperature T dependence of the dimensionless figure of merit zT for a series of $Al_{69-0.75x}Si_{7.5}Cu_xRu_{23.5-0.25x}$ ($x = 0$–8) as well as a previously investigated sample [19] and (b) calculated zT at 500 K as a function of the number of holes per unit cell h assuming $\kappa_{\rm lat} = 1\ {\rm W\,m^{-1}\,K^{-1}}$, an electronic diffusion constant of 0.39 $\rm cm^2\ s^{-1}$, and E_g shown in Fig. 3(c) together with experimental zT values.

minimum $\kappa_{\rm min} \approx 0.76 n^{2/3} k_{\rm B} v_{\rm s} = 0.8\ {\rm W\,m^{-1}\,K^{-1}}$, based on the diffusion-mediated thermal transport theory [30], which could be valid for quasicrystals and quasicrystalline approximants. Although the $\kappa_{\rm lat}$ is lower than $\kappa_{\rm min}$ above 600 K, it is difficult to discuss this underestimated $\kappa_{\rm lat}$ quantitatively. For this point, once we obtain the refined structural model in the future, we would like to quantitatively evaluate the $\kappa_{\rm lat}$ using anharmonic phonon calculations and discuss the unique scattering process.

Figure 6(a) shows zT as a function of T for $Al_{69-0.75x}Si_{7.5}Cu_xRu_{23.5-0.25x}$ ($x = 0$–8) as well as the previously investigated sample. We note that since this approximant is cubic, the anisotropy does not need to be considered. Owing to the carrier doping, zT of all the Cu-doped samples showed a higher value than that of the previously investigated sample over the entire investigated T range. Finally, h was optimized in the $x = 4$ sample, and the maximum zT was improved by a factor of about 6.7, from 0.03 at 400 K in the undoped sample to 0.2 at 500 K. The Al–Si–Ru 1/0 quasicrystalline approximant, which has a low $\kappa_{\rm lat}$ even at room temperature and a narrow E_g of below 0.15 eV, was found to have an optimized zT at a relatively low temperature of 500 K. Figure 6(b) shows the calculated zT at 500 K as a function of the number of holes per unit cell h assuming $\kappa_{\rm lat} = 1\ {\rm W\,m^{-1}\,K^{-1}}$, an electronic diffusion constant $d_{\rm el}$ of 0.39 $\rm cm^2\ s^{-1}$ and E_g shown in Fig. 3(c) together with the corresponding experimental value for each sample. Here the $d_{\rm el}$ was determined in our previous study by fitting the experimental electrical conductivity $\sigma_{\rm expt}$ for undoped sample with the calculated electrical conductivity $\sigma_{\rm calc}$ using the electronic structure obtained by DFT with the $d_{\rm el}$ as a fitting parameter, where $\sigma_{\rm calc}$ is dependent on T, h, and $d_{\rm el}$, i.e., $\sigma_{\rm calc} = \sigma_{\rm calc}(T, h, d_{\rm el})$. Here h was determined by fitting the experimental Seebeck coefficient $S_{\rm expt}$ with the calculated Seebeck coefficient $S_{\rm calc}$, where $S_{\rm calc}$ is dependent on T and h, i.e., $S_{\rm calc} = S_{\rm calc}(T, h)$. Then, fixed h, $d_{\rm el}$ was determined by fitting σ. We note that $d_{\rm el}$ was assumed to be the same value for all samples because the crystal structure of this approximant contains a significant amount of disorder even in the undoped sample, and its relaxation time is extremely short in nature. The calculated zT for $E_g = 0.15$ eV was estimated to increase up to ≈ 0.4 at 500 K by optimizing $h \approx 0.15$. As E_g decreased, the maximum zT decreased, which shifted the optimum h to higher values. Therefore, the maximum $zT\,(= 0.2)$ obtained in this work, which was approximately half of the prediction under the condition of $E_g = 0.15$ eV, arose from the decrease in E_g caused by Cu doping. Future work will be to find elements that can dope carriers while maintaining the magnitude of E_g for further improvement of zT.

IV. SUMMARY

The thermoelectric properties of semiconducting quasicrystalline approximants $Al_{69-0.75x}Si_{7.5}Cu_xRu_{23.5-0.25x}$ ($x = 0, 2, 4, 6, 8$) were investigated in the temperature range of 350 to 800 K. The doped Cu atoms partly behave as hole dopants and improve the thermoelectric performance. In all samples, zT was a maximum at less than 500 K, which indicates that the semiconducting quasicrystalline approximant could be a suitable candidate as a thermoelectric material for low grade waste heat recovery.

ACKNOWLEDGMENT

This work was supported by JSPS KAKENHI under Grants No. JP19H05818 and No. JP19J21779.

[1] A. L. Pope, T. M. Tritt, M. A. Chernikov, and M. Feuerbacher, Appl. Phys. Lett. **75**, 1854 (1999).

[2] A. Bilušić, D. Pavuna, and A. Smontara, Vaccum **61**, 345 (2001).

[3] K. Kirihara and K. Kimura, J. Appl. Phys. **92**, 979 (2002).

[4] T. Nagata, K. Kirihara, and K. Kimura, J. Appl. Phys. **94**, 6560 (2003).

[5] Y. K. Kuo, J. R. Lai, C. H. Huang, C. S. Lue, and S. T. Lin, J. Phys.: Condens. Matter **15**, 7555 (2003).
[6] T. Takeuchi, T. Otagiri, H. Sakagami, T. Kondo, U. Mizutani, and H. Sato, Phys. Rev. B **70**, 144202 (2004).
[7] Y. K. Kuo, K. M. Sivakumar, C. R. Lin, C. S. Lue, and S. T. Lin, J. Appl. Phys. **97**, 103717 (2005).
[8] J. T. Okada, T. Hamamatsu, S. Hosoi, T. Nagata, and K. Kimura, J. Appl. Phys. **101**, 103702 (2007).
[9] Y. Takagiwa, T. Kamimura, S. Hosoi, J. T. Okada, and K. Kimura, J. Appl. Phys. **104**, 073721 (2008).
[10] Y. Takagiwa, T. Kamimura, S. Hosoi, and K. Kimura, Z. Kristallogr. - Cryst. Mater. **224**, 21 (2009).
[11] Y. Takagiwa, T. Kamimura, S. Hosoi, J. T. Okada, and K. Kimura, Z. Kristallogr. - Cryst. Mater. **224**, 79 (2009).
[12] Y. Takagiwa and K. Kimura, Sci. Technol. Adv. Mater. **15**, 044802 (2014).
[13] Y. Iwasaki, K. Kitahara, and K. Kimura, J. Alloys Compd. **763**, 78 (2018).
[14] K. Kitahara, Y. Takagiwa, and K. Kimura, Mater. Trans. **60**, 2490 (2019).
[15] Y. Iwasaki, K. Kitahara, and K. Kimura, Mater. Trans. **61**, 2079 (2020).
[16] Y. Iwasaki, K. Kitahara, and K. Kimura, J. Alloys Compd. **851**, 156904 (2021).
[17] K. Kitahara and K. Kimura, Mater. Trans. **62**, 149 (2021).
[18] J. O. Sofo and G. D. Mahan, Phys. Rev. B **49**, 4565 (1994).
[19] Y. Iwasaki, K. Kitahara, and K. Kimura, Phys. Rev. Mater. **3**, 061601(R) (2019).
[20] A. P. Tsai, Sci. Technol. Adv. Mater. **9**, 013008 (2008).
[21] D. Kapusha, B. Grushko, and T. Y. Velikanovaa, J. Alloys Compd. **493**, 99 (2010).
[22] B. Grushko, J. Gwóźdź, and M. Yurechko, J. Alloys Compd. **305**, 219 (2000).
[23] K. Sugiyama, T. Kato, K. Saito, and K. Hiraga, Philos. Mag. Lett. **77**, 165 (1998).
[24] S. Takahashi, H. Muta, K. Kurosaki, and S. Yamanaka, J. Alloys Compd. **493**, 17 (2010).
[25] A. L. Bail, Powder Diffr. **20**, 316 (2005).
[26] F. Izumi and K. Momma, Solid State Phenoma **130**, 15 (2007).
[27] P. Blaha, G. Madsen, K. Schwarz, D. Kvasnicka, and J. Luitz, *WIEN2k, An Augmented Plane Wave + Local Orbitals Programs for Calculating Crystal Properties, Vol. 1* (Vienna University of Technology Institute of Materials Chemistry, Vienna, 2017).
[28] F. S. Galasso, *Structure and Properties of Inorganic Solids: A Volume in International Series of Monographs in Solid State Physics* (Pergamon, Oxford, UK, 1970).
[29] See Supplemental Material at http://link.aps.org/supplemental/10.1103/PhysRevMaterials.5.125401 for the detail information of the validity of the doped Cu site, calculated model, and nominal compositions of samples.
[30] M. T. Agne, R. Hanus, and G. J. Snyder, Energy Environ. Sci. **11**, 609 (2018).